Sensors and Actuators B 257 (2018) 594–601

Contents lists available at ScienceDirect

Sensors and Actuators B: Chemical

journal homepage: www.elsevier.com/locate/snb

Research paper

Biosensor platform for parallel surface plasmon-enhanced epifluorescence and surface plasmon resonance detection

Agnes T. Reiner, Stefan Fossati, Jakub Dostalek*

BioSensor Technologies, AIT-Austrian Institute of Technology GmbH, Muthgasse 11, 1190 Vienna, Austria

ARTICLE INFO

Article history:
Received 27 June 2017
Received in revised form
15 September 2017
Accepted 20 October 2017
Available online 28 October 2017

Keywords:
Surface plasmon resonance
Plasmon enhanced fluorescence
Epifluorescence
Biosensor

ABSTRACT

For the first time, plasmonic diffraction grating is implemented for the combined direct and epifluorescence-based readout of assays in real-time. This plasmonic structure serves for grating-coupled surface plasmon resonance (SPR) monitoring of molecular binding-induced changes in the refractive index. In parallel, it allows to simultaneously perform plasmonically enhanced fluorescence (PEF) analysis of affinity binding of molecules that are labeled with fluorophores. This configuration offers facile readout of e.g. magnetic nanoparticle-enhanced assays which is not possible with more conventional Kretschmann geometry. The performance characteristics of this combined approach are discussed by using two types of assays. In the first assay a fluorophore-labeled protein with a medium molecular weight of 55 kDa was affinity captured on the plasmonic sensor grating. The associated PEF signal in this assay showed a signal-to-noise ratio that was 140-fold higher compared to that of the SPR detection channel. In the second assay, extracellular vesicles were detected by using antibodies against CD81 attached to the plasmonic grating. These vesicles were pre-concentrated by their coupling to magnetic nanoparticles with cholera toxin B chain. This assay exploited magnetic nanoparticles as labels enabling rapid collection of analyte at the sensor surface and for the enhancement of the SPR sensor response. In this case the label-free SPR detection channel outperformed the fluorescence-based detection, as the SPR signal-to-noise ratio was 2.4-fold higher than that of PEF.

1. Introduction

Fluorescence is a widely used method in bioassays for sensitive detection of chemical and biological species. In order to advance their sensitivity, the fluorophores that are used as labels can be exposed to the confined field of surface plasmons [1,2]. These optical waves are resonantly excited at surfaces of metallic films and metallic nanoparticles and they originate from coupled collective oscillations of the charge density and the associated electromagnetic field. The combination of a surface plasmon-enhanced excitation rate at the fluorophore absorption wavelength, directional surface plasmon-coupled emission at the fluorophore emission wavelength, and an improved quantum yield was demonstrated to enhance the detected fluorescence intensity by a factor up to 10^3 [3]. Such interaction with the intense and confined surface plasmon field was exploited for amplification of the fluorescence signal associated to the affinity binding of labeled analyte biomolecules in bioassays and biosensors in order to improve their performance characteristics [4,5].

Besides plasmon-enhanced fluorescence (PEF) assays, the probing of molecular binding by surface plasmons allows for direct label-free detection of analytes. In surface plasmon resonance (SPR) biosensors, the affinity binding of analyte molecules increases the refractive index at a metallic sensor surface, which detunes the resonant coupling of light to surface plasmons and thus can be optically monitored as a shift of SPR. This method became an established tool in biomolecular interaction studies [6] and it is pursued for rapid and sensitive detection of chemical and biological analytes [7].

The possibility of parallel detection of SPR and PEF holds potential for more advanced detection schemes and molecular interaction studies. Up to now, the attenuated total reflection geometry (ATR) was dominantly used for the excitation of surface plasmons and it has been utilized for the combined SPR and PEF studies. It was reported for the SPR observation of functional biointerfaces combined with enhanced sensitivity of fluorescence-based detection of low molecular weight analytes [8] or biomolecules present at minute concentrations in complex samples [9,10]. In addition, SPR and PEF was employed in the analysis of interaction

* Corresponding author.
E-mail address: jakub.dostalek@ait.ac.at (J. Dostalek).

https://doi.org/10.1016/j.snb.2017.10.116

between DNA polymerase, short oligonucleotide strands attached to a substrate, and labeled nucleotides that formed DNA duplexes [11]. Furthermore, the combination of fluorescence detection of enzyme linked immunoassays and SPR in a single instrument was demonstrated to be suitable for the analysis of target analytes over a broad dynamic range [12].

According to the knowledge of the authors, the combined SPR and PEF readout was implemented up to now only by using ATR configuration. The metallic diffraction grating-coupled SPR on periodically corrugated metallic surfaces provides an alternative means for the excitation and interrogation of surface plasmons, which found its applications in SPR biosensors [13] as well as in PEF detection in *epi*-fluorescence geometry configurations [14,15]. With respect to sensors utilizing ATR, diffraction gratings offer the advantage of simpler use that does not require optical matching of a sensor chip to a prism and it can be exploited in a format compatible with regular (fluorescence) microscopes. In addition, it was shown to enable the utilization of magnetic nanoparticle (MNP)-enhanced assays when a magnetic field gradient can be efficiently applied through a sensor chip in order to overcome diffusion-limited affinity binding kinetics and rapidly collect the pre-concentrated analyte at the sensor surface [16,17].

This work reports on SPR and PEF signal detection based on diffraction grating-coupled SPR and the epifluorescence geometry, which was not reported yet. We demonstrate that such a system can in parallel directly detect binding of biomolecules to the surface via SPR monitoring as well as by PEF when fluorophore labels are used. The performance characteristics of PEF and SPR modalities are investigated for the direct detection of medium size protein molecules and for MNP-enhanced analysis of larger extracellular vesicles (EVs).

2. Experimental

2.1. Materials

Positive photoresist Microposit S1805 was purchased from Shipley and its developer AZ 303 was acquired from Micro-Chemicals. Polydimethylsiloxane elastomer (PDMS) Sylgard 184 was obtained from Dow Corning and the UV-curable polymer Amonil MMS 10 was from AMO GmbH. Dithiolalkanearomatic PEG3 with hydroxyl endgroup (SPT-0013) and the dithiolalkanearomatic PEG6 with carboxyl endgroup (SPT0014A6) were purchased from SensoPath Technologies. N-(3-dimethylaminopropyl)-N'-ethylcarbodiimide hydrochloride (EDC), N-hydroxysuccinimide (NHS), ethanolamine and ethylenglycol, as well as acetic acid and sodiumacetate for the preparation of acetate buffer were bought from Sigma-Aldrich. Phosphate buffered saline (PBS) at a pH of 7.4 from Merck was used for the functionalization steps. PBS with addition of 0.05 % Tween 20 (Sigma-Aldrich) and 0.1 % bovine serum albumine (Thermo Fisher Scientific) (PBSTB) were used as running buffers in all detection experiments. The biotinylated mouse antibody (MG2b-57) was obtained from BioLegend and the mouse monoclonal antibody against human CD81 (1.3.3.22) from Santacruz Biotechnology. Streptavidin was from Thermo Fisher Scientific. Cholera toxin b-chain (CTB) from SBL Vaccin AB was biotinylated with EZ-link Sulfo-NHS-LC-Biotin (Thermo Fisher Scientific) and in parallel fluorescently labeled with Alexa Fluor 647 NHS ester (Thermo Fisher Scientific). MNPs with a diameter of 200 nm conjugated with streptavidin (fluidMAG-Streptavidin) were purchased from Chemicell. Prior to the use, streptavidin-coated MNPs were washed twice with PBSTB by applying a magnetic field for separation of the MNPs from the solution. EVs were generously provided from Sai Kiang Lim's group and their production and purification is described elsewhere [18].

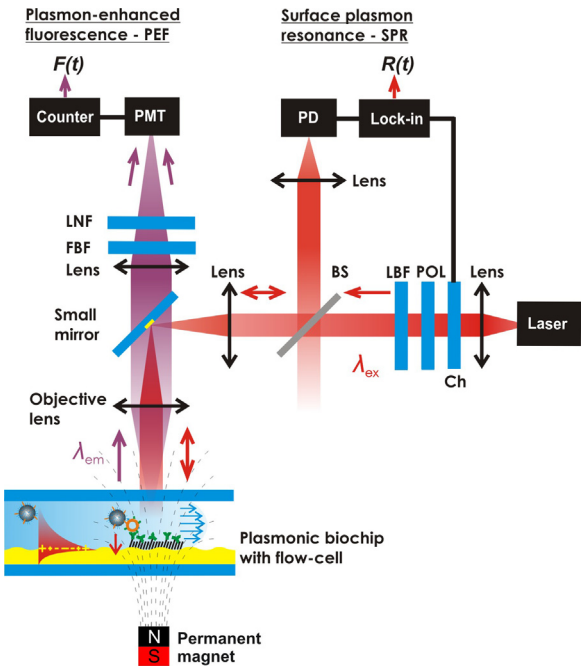

Fig. 1. Schematics of the platform for parallel surface plasmon-enhanced fluorescence and surface plasmon resonance detection (Ch – chopper, POL – polarizer, LBF – laser band-pass filter, BS – beam splitter, FBF – fluorescence band-pass filter, LNF – laser notch filter, F(t) – fluorescence readout, $R(t)$ – SPR readout, PD – photodiode, PMT – photomultiplier).

2.2. Sensor chip preparation

A crossed relief grating was prepared by UV laser interference lithography and their multiple copies were made by soft lithography as described before [15]. Briefly, the used structure comprised of two superimposed crossed sinusoidal modulations with a period of Λ = 434 nm. The structure was cast to PDMS, which was cured over night at 60 °C before it was used as a working stamp. Cleaned BK7 glass substrates were coated with the UV-curable polymer Amonil MMS 10 by spin-coating at 3000 rpm for 120 s. Then, the PDMS working stamp was placed on the top of the Amonil layer and the structure cast to this polymer was irradiated by UV light (UV lamp Bio-Link 365, Vilber Lourmat). Finally, the PDMS stamp was detached from the cured Amonil MMS 10 leaving a copy of the master structure on the glass substrate. The grating copies were subsequently coated with 4 nm of chromium and 100 nm of gold by vacuum thermal evaporation (HHV AUTO 306 from HHV LTD) in vacuum better than 10^{-6} mBar. Each sensor chip consisted of an area with grating structure and an area with plain gold that was used for control measurements.

2.3. Optical system

The used optical system for the *in situ* detection of diffraction grating-coupled SPR and PEF was adopted based on our previous work [15] and it can be seen in Fig. 1. A beam emitted from a He-Ne laser (power of about 2 mW) at λ_{ex} = 633 nm subsequently travelled through a chopper, polarizer and laser band-pass filter (LBP, FL632.8-10 from Thorlabs). Then it passed through a beam splitter and it was focused by a lens (AC-254-040) on a mirror of 2 mm diameter, consisting of a 100 nm thick gold layer deposited on a BK7 glass slide. The mirror was oriented at 45 deg with respect to the incident beam. A lens (AC-254-040) collimated the reflected beam towards the sensor surface with relief gold diffraction grating mounted in its focal distance. A flow-cell was clamped to the gold sensor chip surface in order to contain aqueous samples. The flow-

cell comprised of a flow chamber with a volume of ~50 μL defined by a PDMS gasket and a transparent fused silica glass substrate with inlet and outlet ports. Upon its incidence at the gold grating surface, the laser beam at λ_{ex} was partially coupled to surface plasmons propagating along the gold surface and partially reflected. The reflected beam was focused back on the mirror by the objective lens and its intensity was detected by using a beam splitter and a photodiode connected to a lockin amplifier (7260 from EG&G). These means allowed the measurement of the detuning of SPR associated to the binding-induced refractive index variations. In addition, the enhanced field intensity at λ_{ex} was employed for the excitation of Alexa Fluor 647 (AF647) fluorophores that we used as labels in the fluorescence assays. The enhanced directional surface plasmon-coupled emission at λ_{em} = 670 nm was collimated by the objective lens, passed around the small mirror and was focused by a lens (AC-254-080, Thorlabs) to a photomultiplier (H6240-01, Hamamatsu) that was connected to a counter (53131A from Agilent). In order to separate light at the excitation wavelength λ_{ex} and the fluorescence beam at λ_{em}, a set of filters was used consisting of a notch filter (XNF-632.8-25.0 M from CVI Melles Griot) and two bandpass filters (FB670-10 from Thorlabs and 670FS10-25 from Andover Corporation Optical Filter). The output from the counter was recorded in counts per second (cps) by using software Wasplas developed at Max Planck Institute for Polymer Research in Mainz (Germany). It is worth of noting that the used implementation of SPR measurements allowed for measurements of bulk refractive index changes as small as 3×10^{-4} RIU. This value was determined as the ratio $\Delta n/(\sigma(R)/\Delta R_B)$ where $\sigma(R) = 3.6 \times 10^{-3}$ a.u. is the standard deviation of the reflectivity signal $R(t)$ and ΔR_B refers to the reflectivity change induced by the refractive index increase Δn due to the pumping of PBS spiked with 2 % ethylenglycol through the flow cell.

In the MNP-enhanced assays, a gradient magnetic field ∇B was applied through the sensor chip. A cylindrical permanent magnet (NdFeB with diameter of 10 mm and length of 35 mm from Neotexx) was approached to the grating sensor chip in order to expose its surface to the field gradient of about $\nabla B = 0.10\,\mathrm{T\,mm^{-1}}$ [16]. By removing the magnet, the magnetic field gradient was switched off to $\nabla B = 0$.

2.4. Functionalization of sensor chips

The gold surface of the sensor chips was immersed in a 1 mM thiol solution in ethanol in order to form a mixed self-assembled monolayer (SAM). The solution comprised of a mixture of dithiol-PEG6 with carboxyl end group for later surface functionalization and dithiol-PEG3 with hydroxyl end group in order to form an antifouling background. The molar ratio of carboxyl to hydroxyl-terminated thiols was 1:9. After the overnight incubation, the sensor chips were thoroughly rinsed with ethanol, dried immediately in a stream of air and stored under argon gas.

The immobilization of either biotinylated unspecific antibodies or unconjugated specific antibodies against CD81 was performed *in situ* by amine coupling according to standard protocols. All solutions were flowed over the sensor surface at a constant speed of 45 μL/min. As a first step PBS was rinsed through the flow cell to reach a stable baseline in SPR signal. In order to calibrate the sensor, PBS spiked with 2 % ethylenglycol was flowed through, triggering a refractive index change of 2×10^{-3} refractive index units (2 mRIU). Afterwards, sodium acetate buffer with a pH-value of 5 was rinsed to adjust the pH for the consecutive amine coupling. The carboxyl groups on the surface were activated by flowing a mixture of 0.4 M EDC and 0.2 M NHS in water for 15 min. After rinsing the surface with sodium acetate buffer, the antibody, diluted in the same buffer at a concentration of 25 μg/mL, was flowed for 10 min. Finally, ethanolamine at 1 M and pH of 8.5 was used to inactivate all remaining carboxyl groups before the buffer was changed again to PBS.

2.5. Direct detection bioassay

Unspecific biotinylated antibodies were immobilized on the sensor surface by amine coupling and followed by the affinity binding of streptavidin and a fluorescently labeled biotin-CTB conjugate (see Fig. 2a). In these measurements PBSTB was used as running buffer and flowed over the sensor surface at a constant speed of 45 μL/min. First streptavidin at a concentration of 5 μg/mL diluted in PBSTB was rinsed across the surface for 10 min. After washing with PBSTB, the biotinylated CTB that was also labeled with AF647 was pumped through the flow-cell at a concentration of 5 μg/mL.

2.6. Magnetic nanoparticle-enhanced bioassay

The MNP-enhanced bioassay for EV detection was performed as described in our previous work [17] with the addition of the AF647 labeling of the lipid-binding protein CTB. Briefly, 3 μg of mesenchymal stem cell-derived EVs were incubated with 250 ng of biotinylated and AF647-labeled CTB for 30 min at room temperature on a shaker. Then 10 μg of washed MNPs capped with streptavidin were added to the sample and incubated again at the same conditions (see Pre-incubation in Fig. 2b). Afterwards, the MNPs with bound EVs were washed twice with PBSTB and finally re-suspended in 1 mL buffer, leading to a concentration estimate of 3 μg total protein amount of vesicles per mL PBSTB or 520 fM based on the particle count determined by nanoparticle tracking analysis of the input EV sample. As control sample the MNPs were incubated only with the biotinylated and fluorescently labeled CTB. Then the control MNPs or MNP-bound EVs were collected on the sensor surface, which was first functionalized with antibodies specific for CD81, by rinsing the samples across the surface while a magnetic field gradient $\nabla B = 0.10\,\mathrm{T\,mm^{-1}}$ was applied (see Affinity binding in Fig. 2b). After a 10 min incubation the magnetic field gradient was switched off $\nabla B = 0$ and the sensor surface was washed with

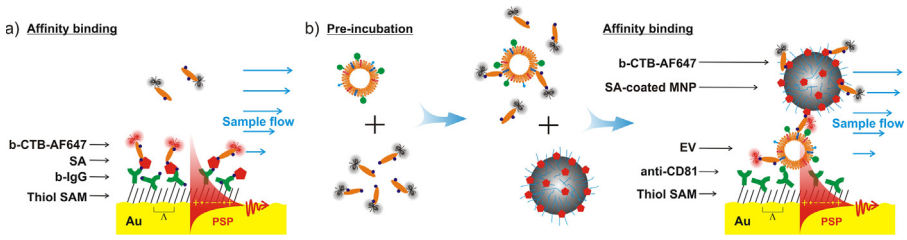

Fig. 2. Schematics of the assays used for testing of the sensing platform. a) The detection assay of medium sized CTB protein based on biotin-streptavidin affinity binding and fluorescent labeling with AF647. b) Extracellular vesicle (EV) assay consisting of the pre-incubation step and collection of the EVs at the sensor surface (MNPs – magnetic nanoparticles, b-CTB-AF647 – biotinylated cholera toxin b-chain conjugated with Alexa Fluor 647, SA – streptavidin, b-IgG – biotinlyated unspecific antibody, anti-CD81 – specific antibody for CD81, SAM – self assembled monolayer, Au – gold, PSP – propagating surface plasmon, Λ – period).

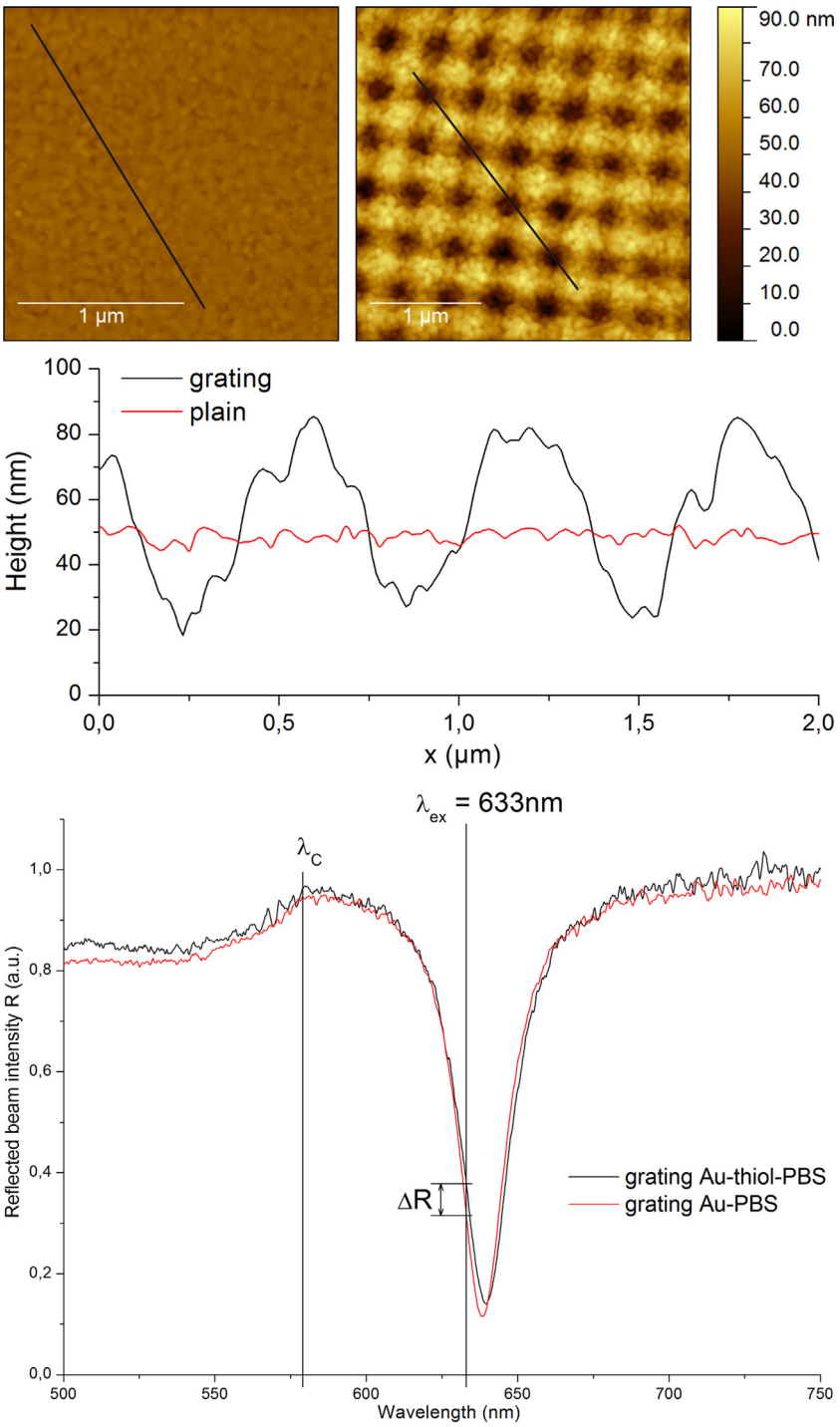

Fig. 3. a) Atomic force microscopy image of the plain (left) and grating (right) sensor surface after the coating with gold (scale bar corresponds to 1 µm). b) Height profiles of the plain and grating sensor surface of the indicated black lines in a). c) Wavelength reflectivity spectra for a normally incident beam at the sensor chip with a clamped flow-cell that was flooded with PBS before and after deposition of a mixed thiol SAM. The reflectivity change ΔR at a fixed wavelength of λ_{ex} = 633 nm is indicated.

PBSTB for 20 min. Due to the architecture of the setup and flow-cell, flushing shortly with running buffer at high speed was necessary to remove any unspecifically attached MNPs and aggregates.

3. Results and discussion

3.1. Characterization of GC-SPR sensor chips

The prepared sensor chip with or without the crossed grating corrugation carried a conformal 100 nm thick gold film. Atomic force microscopy of these surfaces presented in Fig. 3a and b reveal that the periodicity of the two overlaid crossed sinusoidal modulations on grating area was about the targeted Λ = 434 nm, and the corrugation depth was 60 nm. This corrugation depth corresponds to the amplitude of the sinusoidal modulation in each perpendicular direction of about 15 nm. This value was showed before to be optimum for strong diffraction coupling to propagating surface plasmons (PSP) in the red part of the spectrum at an interface between gold and water [13]. The wavelength reflectivity spectra of the grating structured sensor chip, which was clamped to a flow-

cell and flooded with PBS buffer, was measured by using a system reported before [17]. As visible in Fig. 3c, a narrow dip in the reflectivity spectrum occurs at the wavelength λ_{SPR} = 638 nm due to the first diffraction order excitation of PSPs on a periodically corrugated surface. The resonant wavelength λ_{SPR} can be controlled by varying the period Λ which was chosen in order to tune λ_{SPR} slightly above the excitation wavelength λ_{ex} = 633 nm that is further used in fluorescence measurements. After forming a mixed thiol SAM at the gold surface, the SPR shifts to a longer wavelength of λ_{SPR} = 639 nm due to the increase in the refractive index, as shown in Fig. 3c. The resonance wavelength shift of about 1 nm corresponds to the adlayer thickness of ~1 nm [19] which indicates that a compact mixed thiol SAM layer was formed on the gold surface. For the normally incident beam at λ_{ex} this shift is manifested as an increase in the reflectivity ΔR as its wavelength is coincident with the edge of the resonance dip.

In the further experiments, the gold grating structure was used for observing affinity binding events in two modes in parallel by using the optical setup showed in Fig. 1. Firstly, the direct SPR observation of molecular binding was implemented by measuring the reflectivity ΔR changes. An increase in the refractive index is manifested as a red shift in the SPR wavelength λ_{SPR} which is accompanied with an increase in the reflectivity at the chosen wavelength λ_{ex} (tuned to the edge of the resonance). Secondly, the enhanced intensity of the electromagnetic field associated with the resonance excitation of PSPs at λ_{ex} increases the excitation rate of AF647-labeled molecules bound to the surface. In addition, the same structure allows to exploit directional surface plasmon-coupled emission at the AF647 emission wavelength λ_{em} = 670 nm. The combination of these two effects offers means for the amplification of the fluorescence – PEF – signal $F(t)$ and *in situ* fluorescence monitoring of affinity binding events at the sensor surface [20]. Our previous work on PEF exploiting a similar grating configuration demonstrated an enhanced collection yield of emitted fluorescence photons at λ_{em} by a factor ~ 4 and about 40-times increased excitation rate at λ_{ex} with respect to a flat gold film [15]. Concerning the leakage losses to the substrate, we assume those are negligible as the fluorescence occurs on a gold film with a thickness of about 100 nm.

Two assays are carried out in order to demonstrate the performance of dual SPR and PEF readout and compare the sensitivity of these two detection modalities. Firstly, the combined SPR and PEF detection was used for the affinity binding of protein molecules in the close proximity to the gold sensor surface. Secondly, the implementation of SPR and PEF measurements for the detection of extracellular vesicles – EVs – is pursued with the aid of magnetic nanoparticles – MNPs – that allow for the efficient collection of such analytes at the sensor surface by application of a magnetic field gradient ∇B. For both experiments and readout modalities sensor chips with a plasmonic grating and a reference flat gold film were used.

3.2. Observation of affinity binding of protein analyte

Fig. 4 shows the SPR and PEF sensorgrams measured upon the preparation of the sensor surface architecture as well as for the affinity binding of biotinylated cholera toxin b chain (b-CTB). As seen in Fig. 2a, the surface of the sensor chip was functionalized with streptavidin (SA) and an additional layer of biotinylated antibody (b-IgG) was used between the gold surface and the SA layer in order to avoid the fluorescence quenching (that occurs at distances <15 nm due to the Förster energy transfer [21]). The acquired sensorgrams include the fluorescence signal $F(t)$ and SPR reflectivity changes $\Delta R(t)$. For comparison, the molecular binding experiments were performed at two areas on the sensor chip: Fig. 4a shows the

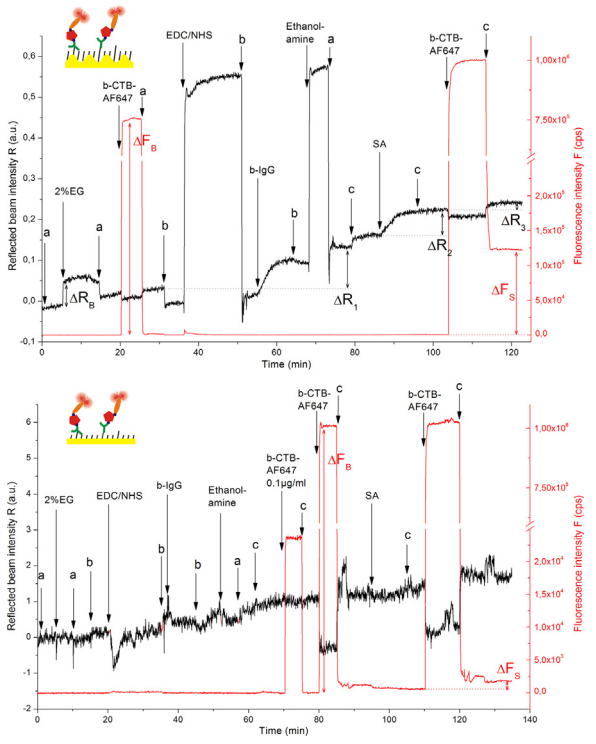

Fig. 4. SPR signal $R(t)$ and fluorescence signal $F(t)$ during amine coupling of a biotinylated unspecific antibody (b-IgG) and affinity binding of fluorescently labeled and biotinylated cholera toxin b-chain (b-CTB-AF647) on a grating gold chip (a) and a reference plain gold chip (b) as control. Insets on the top left show pictograms of the assay and the respective surface used. The signal responses to the affinity binding of molecules at the surface are indicated as ΔR or ΔF for SPR and fluorescence, respectively (a – PBS, b – acetate buffer pH = 5, c – PBSTB, EG – ethylenglycol, b-IgG dissolved at 25 µg/mL, SA – streptavidin at 5 µg/mL).

sensor response at the grating surface and Fig. 4b at a reference flat area (where SPR is not generated).

Firstly, a baseline in the reflectivity $\Delta R(t)$ and fluorescence $F(t)$ signal was established upon a flow of PBS. Then, a PBS solution spiked with 2 % ethylene glycol was injected, followed by rinsing with PBS. This step was used to calibrate the SPR sensor channel by using the bulk refractive index change above the sensor surface which corresponds to about $\Delta n = 2 \times 10^{-3}$ refractive index units (RIU). The initial increase in the baseline signal, seen in Fig. 4a, didn't affect the results, because only the bulk change was used, and later the signal stabilized. As can be seen in Fig. 4a, this increase in the refractive index (t = 5–15 min) caused a change in the SPR signal ΔR_B = 0.06 a.u. on a grating surface and no response was observed on a reference flat gold film (as presented in Fig. 4b). Similarly, the fluorescence detection channel was tested by a flow of b-CTB carrying AF647 tags (dissolved at a concentration of 5 µg/mL) over the gold grating (Fig. 4a, t = 20-25 min) and on a flat gold surface (Fig. 4b, t = 80–85 min) that did not carry SA moieties. A similar fluorescence signal increase in the range of $\Delta F_b = 0.75–1 \cdot 10^6$ cps was measured on both areas due to the excitation of fluorophores present in the bulk solution. The fluorescence signal F rapidly dropped back to the original baseline after the rinsing with PBS which indicates weak unspecific sorption to the surface.

Both grating and flat gold areas on the sensor chip were modified by b-IgG with the use of amine coupling followed by affinity binding SA. Fig. 4a shows the obtained sensorgram on a grating surface for the activation of carboxyl groups by a mixture of EDC/NHS (t = 35–50 min), covalent binding of b-IgG (t = 55–65 min), passivation of unreacted carboxyl groups with ethanolamine (t = 70–75 min), and binding of SA (t = 85–95 min). The same sequence and incubation times were performed in the

flat area on the sensor chip and respective sensorgrams are presented in Fig. 4b. On the grating surface, the binding of b-IgG and SA increased the reflectivity signal by $\Delta R_1 = 0.10$ a.u. and $\Delta R_2 = 0.06$ a.u., respectively, while no measurable change was observed on a flat gold surface ($t = 20$–105 min). The observed reflectivity changes on the SPR grating area of the sensor chip correspond to the surface mass density of 1.2 ng/mm^2 for IgG and of 0.73 ng/mm^2 for SA which is comparable to values reported in literature [22,23].

After the immobilization of b-IgG and SA, a solution with CTB conjugated with biotin and AF647 tags (b-CTB-AF647, concentration of 5 μg/mL) was flowed over the sensor surface for 10 min. On both grating area (Fig. 4a, $t = 105$–115 min) and reference flat area (Fig. 4a, $t = 110$–120 min) a weak drop in the reflectivity $R(t)$ occurs due to the absorption of the excitation light by fluorophores dissolved in the bulk solution. However, after the rinsing with buffer an increase in reflectivity of $\Delta R_3 = 0.02$ a.u. was measured on a grating while no measurable change occurred on a reference flat gold area. The SPR reflectivity response on the grating area due to b-CTB-AF647 binding showed a signal-to-noise ratio of $\Delta R_3/\sigma(R) \sim 5$. Contrary to the reflectivity measurement, the fluorescence detection channel $F(t)$ showed a much more pronounced signal. After the injection of b-CTB-AF647 a rapid increase in $F(t)$ is observed due to the dominant excitation of fluorophores in the bulk solution. After the 10 min incubation, the surface was rinsed with PBSTB and a strong change in fluorescence signal ΔF_S caused by the affinity binding becomes visible. The fluorescence change yields $\Delta F_S = 1.22 \times 10^5$ cps on the grating area and $\Delta F_S = 1.2 \times 10^3$ cps on the reference flat area. The associated signal-to-noise ratio of fluorescence response on the grating area was ~700. Hence, the accuracy of PEF readout outperforms the SPR on the grating surface by more than two orders of magnitude. Besides allowing for dual fluorescence and SPR detection, the used plasmonic grating enhanced the fluorescence signal originating from the grating surface compared to the flat surface by a factor of ~100, which agrees with earlier published simulations and measurements of PEF using epifluorescence geometry [15].

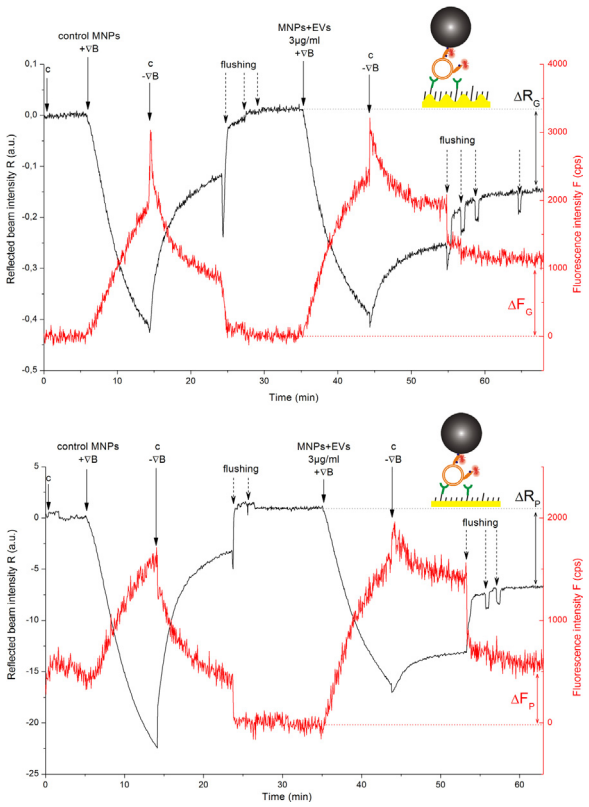

Fig. 5. SPR signal $R(t)$ and fluorescence signal $F(t)$ of a magnetic nanoparticle (MNP)-enhanced assay measurement on a grating gold chip (a) and a reference plain gold chip (b) as control. Insets on the top right show pictograms of the assay and the respective surface used. The application of the magnetic field for collection of MNPs and bound extracellular vesicles (EVs) is indicated as "$+\nabla B$" and its removal as "$-\nabla B$". The signal responses to the affinity binding of molecules to the surface are indicated as ΔR or ΔF for SPR and fluorescence, respectively (c – PBSTB).

3.3. *Magnetic nanoparticle-enhanced observation of affinity binding of extracellular vesicles*

Since the grating coupled SPR configuration and the epifluorescence geometry for PEF readout use only the front side of the sensor chip, there is free space at the back of the chip and flow-cell. This space was used for the applying a magnetic field gradient ∇B for the improved collection of the target analyte, that is affinity bound to MNPs, at the sensor surface. As we reported before, this approach allows to overcome the slow diffusion-limited mass transfer of the analyte [16,24]. Hence we incorporated the MNP-enhanced detection assay for EVs [17] into our optical setup for combined detection of SPR and PEF. It is worth of noting that in this second assay the target analyte, EVs, exhibit a larger size of about 100 nm compared to the previous assay in which a protein with a size of about several nanometers was detected.

In a pre-incubation step, the target EV analyte was first bound to MNPs via the lipid binding protein CTB with biotin tags, as illustrated in Fig. 2b. In order to achieve fluorescence detection of the EVs, CTB molecules were additionally labeled with AF647. For affinity binding of EVs at the sensor surface, the grating and reference flat areas were functionalized with antibodies specific for CD81 which is a protein present on the CTB-binding vesicles [18]. The immobilization of the anti-CD81 at the surface was accompanied with an SPR shift of $\Delta R = 0.13$ a.u. corresponding to the surface mass density of 1.6 ng/mm^2 (measured on the structured gold surface, sensorgram not shown), which is similar to the results discussed above.

Firstly PBSTB buffer was flowed over the gold grating (Fig. 5a) and reference flat (Fig. 5b) areas carrying anti-CD81 to establish a baseline ($t = 0$–5 min). Then the sensor surface was exposed to control MNPs in order to test for unspecific binding to the sensor surface (Fig. 5a and b, $t = 5$–15 min). These sensorgrams show that the SPR signal R decreased and fluorescence intensity F increased upon the accumulation of MNPs reacted with CTB-AF647 conjugate at the sensor surface, to which the MNP-CTB-AF647 mix without target EV analyte was pulled by the magnetic field gradient ∇B applied.

Interestingly, the SPR signal decrease is more pronounced on the reference plain gold area of the sensor chip than on that with grating. The reason is that the accumulated MNPs (with the size of about 200 nm) form a layer on the sensor surface that is substantially thicker than the probing depth of PSPs (< 100 nm). Therefore, the decrease in the reflected intensity is mostly due to the scattering and absorption by MNPs. On the flat gold surface the beam passes twice through this layer while on the grating surface only once as the majority of its intensity is transferred to the PSPs. Furthermore, MNPs in contact with the gold surface enhance the refractive index leading to a SPR signal increase R on the grating surface that counteracts the absorption of light intensity by the MNPs. In our previous work on the MNP-enhanced GC-coupled SPR biosensor [17] we monitored the wavelength reflectivity spectra over time and hence were able to discriminate the influence of light absorption and refractive index change occurring in vicinity to the gold surface. However, since we use a monochromatic light source for both fluorescence excitation and SPR measurements, this approach is not applicable for the parallel SPR and PEF measurements. The

Table 1
Comparison of the signal-to-noise ratio obtained for the surface functionalization and the tested assays in the reflectivity and fluorescence channel on grating and plain gold sensing areas.

Assay	Readout type	Grating gold	Plain gold
b-IgG2b immobilization	SPR	23 ± 9[a]	–
Anti-CD81 immobilization	SPR	40 ± 12[b]	–
b-CTB-AF647 detection	SPR	5	–
	Fluorescence	700	18
MNP-enhanced detection of EVs	SPR	44	76
	Fluorescence	18	12

[a] mean and standard deviation over 2 experiments.
[b] mean and standard deviation over 3 experiments.

fluorescence signal change was observed at a similar level both on grating and plain gold as it mostly originates from a distance longer than the PSP probing depth and thus it is not plasmonically amplified.

After switching off the magnetic field gradient ∇B and rinsing the flow-cell with PBSTB (Fig. 5a and b, $t = 15–35$ min) the unbound MNPs were quickly washed away. Due to the architecture of the instrument, flushing of the flow cell with running buffer was required to remove all unbound MNPs. These flushing steps are indicated in the sensorgrams by dashed arrows and present as sharp signal shifts. After flushing, SPR and PEF signals stabilized at the same level as before the MNP incubation, indicating that there was no unspecific binding to the functionalized surfaces.

Next the MNPs pre-incubated with the target EV analyte (at an estimated concentration of 3 μg total protein/mL or 520 fM) and CTB (conjugated with biotin and AF647) were collected at the sensor surface in the same manner as before for the control MNPs (Fig. 5a and b, $t = 35–45$ min). Again a similar decrease in SPR was observable, but after switching off the magnetic field gradient and flushing with PBSTB (Fig. 5a and b, $t = 45–65$ min) a reflectivity change of $\Delta R_G = 0.16$ a.u. on the grating gold area and $\Delta R_P = 7.72$ a.u. on the plain gold area was measured due to the affinity binding of EVs carried by MNPs to immobilized anti-CD81 antibodies. Since a decrease in the reflectivity R is observed on both grating and plain gold surfaces, it can be concluded that mainly the effect of light absorption and scattering by the MNPs is responsible for the signal change. Therefore, on the grating exhibiting SPR the reflectivity increase due to the analyte capture is overrun by the reflectivity decrease due to the MNPs. This counteraction also translates in the signal-to-noise ratio that is 1.7-fold lower for the grating gold (∼44) compared to the plain gold (∼76), see overview in Table 1. Hence the measurement on plain gold, which detects only light absorption by MNPs, performed better. In order to make use of the SPR signal change in addition to the light absorption and thus reaching higher signal-to-noise ratios, the coupling resonance needs to be tuned (e.g. by varying the grating period Λ) in a way that the resonance wavelength λ_{SPR} is shorter than the excitation wavelength λ_{ex}, resulting in a signal decrease upon binding of the target analyte to the sensor surface. It is worth of noting that a similar approach was adopted for the angular modulation of GC-SPR [24].

In the fluorescence channel a signal increase of $\Delta F_G = 1100$ cps and $\Delta F_P = 590$ cps for the grating and the plain gold chip, respectively, were observed due to binding of MNP-bound EVs to the sensor surface. The signal-to-noise ratio of ∼18 on the grating gold and ∼12 on the plain gold was reached with this assay, which implies a small signal improvement for the PSPs coupling with fluorophores. This also translates to the relatively small fluorescence enhancement of only 2-fold by PSPs. There are several explanations for the weak performance of the fluorescence channel for this type of assay. First, the monitored reflected beam intensity indicates that the binding of MNPs to the surface is accompanied with strong light absorption. This absorption likely decreases the intensity of light at the excitation wavelength λ_{ex} as well as at the emission wavelength λ_{em}. The MNP-induced absorption at λ_{ex} leads to a less efficient excitation of PSPs, which again leads to lower levels of fluorescence signal amplification. Similarly for λ_{em} this effect disrupts the surface plasmon-coupled emission. In addition, the fluorescence photons emitted from a volume between gold and MNPs (see Fig. 2b) are partially blocked by these objects on both flat and grating surfaces.

Since the fluorescence enhancement in the grating coupled SPR and PEF sensor is inhibited by the presence of MNPs, a possible solution for signal improvement would be to remove the MNPs after the collection of the target analyte on the sensor surface. This could be achieved by dissociating the binding of the biotinylated CTB molecules and the SA coated MNPs and will be the subject of further studies. One solution could be to use desthiobiotin for the binding of EVs to the SA-MNPs. This type of biotin has a lower affinity to SA and therefore MNPs could be dissociated by replacement of desthiobiotin with biotin [23,25]. As free biotin has a higher affinity to SA compared to surface bound biotin [26], another very similar approach is to replace the biotin that is bound to the MNPs by addition of a high concentration of free biotin in solution. Furthermore, the sensitivity of the MNP-based assay for EV-detection could be improved by exploiting the surface plasmon-enhanced light scattering caused by MNPs, as it was demonstrated by Yang et al. [27].

4. Conclusions

Plasmonic grating was implemented for the combined label-free surface plasmon resonance (SPR) and plasmonically enhanced fluorescence (PEF) measurement of the affinity binding at the sensor surface by using epifluorescence geometry for the first time. These measurements can be performed on the same spot in parallel and in real-time and they allow for facile implementing magnetic nanoparticle-enhanced assays. The monitoring of the affinity binding of a medium sized protein that was labeled with Alexa Fluor 647 dyes showed a ∼100-fold fluorescence enhancement on the gold grating surface compared to a reference flat gold surface. The PEF readout outperformed SPR for this assay when the molecular binding occurs at distances of 15–20 nm from the metallic sensor surface and the respective signal-to-noise ratio was ∼140-fold higher. The reported geometry allows for the incorporation of magnetic nanoparticle (MNP)-enhanced assays for the detection of larger analytes, which exhibit slow diffusion that hinders their affinity binding to the sensor surface. The combined PEF and SPR readout was utilized for the detection of extracellular vesicles (EVs) with the size of about hundred nanometers. The MNPs offered means for efficient delivery and affinity binding of the target EV analyte at the sensor surface, but they substantially hindered the performance of the fluorescence-based assay. The SPR detection channel outperformed the PEF in the MNP-based assay and provided a 2.4-fold higher signal-to-noise ratio. For efficient PEF detection that takes advantage of MNPs, reversible coupling mechanism for the capture of the target analyte on MNPs should be

adopted in order to detach them after the delivery and affinity binding of the target analyte at the sensor surface.

Conflict of interest

None.

Acknowledgments

ATR was supported by the Austrian Federal Ministry for Transport, Innovation and Technology (GZ BMVIT-612.166/0001-III/I1/2010) via the International Graduate School Bio-Nano-Tech – a joint Ph.D. program of the University of Natural Resources and Life Sciences Vienna (BOKU), the Austrian Institute of Technology (AIT), and the Nanyang Technological University (NTU). SF acknowledges support from the European Union's Horizon 2020 Research and Innovation Programme under Grant agreement No. 633937, project ULTRAPLACAD.

References

[1] M. Li, S.K. Cushing, N.Q. Wu, Plasmon-enhanced optical sensors: a review, Analyst 140 (2015) 386–406.
[2] J.R. Lakowicz, K. Ray, M. Chowdhury, H. Szmacinski, Y. Fu, J. Zhang, et al., Plasmon-controlled fluorescence: a new paradigm in fluorescence spectroscopy, Analyst 133 (2008) 1308–1346.
[3] A. Kinkhabwala, Z.F. Yu, S.H. Fan, Y. Avlasevich, K. Mullen, W.E. Moerner, Large single-molecule fluorescence enhancements produced by a bowtie nanoantenna, Nat. Photonics 3 (2009) 654–657.
[4] J. Dostalek, W. Knoll, Biosensors based on surface plasmon-enhanced fluorescence spectroscopy, Biointerphases 3 (2008) Fd12–Fd22.
[5] M. Bauch, K. Toma, M. Toma, Q.W. Zhang, J. Dostalek, Plasmon-Enhanced fluorescence biosensors: a review, Plasmonics 9 (2014) 781–799.
[6] R. Gambari, G. Feriotto, C. Rutigliano, N. Bianchi, C. Mischiati, Biospecific interaction analysis (BIA) of low-molecular weight DNA-binding drugs, J. Pharmacol. Exp. Ther. 294 (2000) 370–377.
[7] J. Homola, Surface plasmon resonance sensors for detection of chemical and biological species, Chem. Rev. 108 (2008) 462–493.
[8] T. Liebermann, W. Knoll, P. Sluka, R. Herrmann, Complement hybridization from solution to surface-attached probe-oligonucleotides observed by surface-plasmon-field-enhanced fluorescence spectroscopy, Colloid Surf. A 169 (2000) 337–350.
[9] Y. Wang, A. Brunsen, U. Jonas, J. Dostalek, W. Knoll, Prostate specific antigen biosensor based on long range surface plasmon-Enhanced fluorescence spectroscopy and dextran hydrogel binding matrix, Anal. Chem. 81 (2009) 9625–9632.
[10] F. Yu, B. Persson, S. Lofas, W. Knoll, Attomolar sensitivity in bioassays based on surface plasmon fluorescence spectroscopy, J. Am. Chem. Soc. 126 (2004) 8902–8903.
[11] G. Stengel, W. Knoll, Surface plasmon field-enhanced fluorescence spectroscopy studies of primer extension reactions, Nucleic Acids Res. 33 (2005) e69.
[12] J. Breault-Turcot, H.P. Poirier-Richard, M. Couture, D. Pelechacz, J.F. Masson, Single chip SPR and fluorescent ELISA assay of prostate specific antigen, Lab Chip 15 (2015) 4433–4440.
[13] J. Dostalek, J. Homola, M. Miler, Rich information format surface plasmon resonance biosensor based on array of diffraction gratings, Sens. Actuators B Chem. 107 (2005) 154–161.
[14] X.Q. Cui, K. Tawa, K. Kintaka, J. Nishii, Enhanced fluorescence microscopic imaging by plasmonic nanostructures: from a 1D grating to a 2D nanohole array, Adv. Funct. Mater. 20 (2010) 945–950.
[15] M. Bauch, S. Hageneder, J. Dostalek, Plasmonic amplification for bioassays with epi-fluorescence readout, Opt. Express 22 (2014) 32026–32038.
[16] Y. Wang, J. Dostalek, W. Knoll, Magnetic nanoparticle-enhanced biosensor based on grating-coupled surface plasmon resonance, Anal. Chem. 83 (2011) 6202–6207.
[17] A.T. Reiner, N.G. Ferrer, P. Venugopalan, R.C. Lai, S.K. Lim, J. Dostalek, Magnetic nanoparticle-enhanced surface plasmon resonance biosensor for extracellular vesicle analysis, Analyst (2017), http://dx.doi.org/10.1039/c7an00469a.
[18] R.C. Lai, S.S. Tan, R.W. Yeo, A.B. Choo, A.T. Reiner, Y. Su, et al., MSC secretes at least 3 EV types each with a unique permutation of membrane lipid, protein and RNA, J. Extracellular Vesicles 5 (2016) 29828.
[19] P. Adam, J. Dostalek, J. Homola, Multiple surface plasmon spectroscopy for study of biomolecular systems, Sens. Actuators B. Chem. 113 (2006) 774–781.
[20] S. Hageneder, M. Bauch, J. Dostalek, Plasmonically amplified bioassay – Total internal reflection fluorescence vs. epifluorescence geometry, Talanta 156–157 (2016) 225–231.
[21] K. Sergelen, S. Fossati, A. Turupcu, C. Oostenbrink, B. Liedberg, W. Knoll, et al., Plasmon field-Enhanced fluorescence energy transfer for hairpin aptamer assay readout, ACS Sens. 2 (2017) 916–923.
[22] J. Voros, The density and refractive index of adsorbing protein layers, Biophys. J. 87 (2004) 553–561.
[23] W. Knoll, M. Zizlsperger, T. Liebermann, S. Arnold, A. Badia, M. Liley, et al., Streptavidin arrays as supramolecular architectures in surface-plasmon optical sensor formats, Colloid Surf. A 161 (2000) 115–137.
[24] Y. Wang, W. Knoll, J. Dostalek, Bacterial pathogen surface plasmon resonance biosensor advanced by long range surface plasmons and magnetic nanoparticle assays, Anal. Chem. 84 (2012) 8345–8350.
[25] J.D. Hirsch, L. Eslamizar, B.J. Filanoski, N. Malekzadeh, R.P. Haugland, J.M. Beechem, Easily reversible desthiobiotin binding to streptavidin, avidin, and other biotin-binding proteins: uses for protein labeling detection, and isolation, Anal. Biochem. 308 (2002) 343–357.
[26] V.H. Perez-Luna, M.J. O'Brien, K.A. Opperman, P.D. Hampton, G.P. Lopez, L.A. Klumb, et al., Molecular recognition between genetically engineered streptavidin and surface-bound biotin, J. Am. Chem. Soc. 121 (1999) 6469–6478.
[27] C.T. Yang, L. Wu, X.H. Liu, N.T. Tran, P. Ba, B. Liedberg, et al., Exploiting surface-Plasmon-Enhanced light scattering for the design of ultrasensitive biosensing modality, Anal. Chem. 88 (2016) 11924–11930.

Biographies

Agnes T. Reiner is a PhD candidate at the University for Natural Resources and Life Sciences in Vienna and the Nanyang Technological University in Singapore. She works at the AIT-Austrian Institute of Technology in Vienna and her research interests are extracellular vesicles, cancer diagnosis, and plasmonic biosensors.

Stefan Fossati is a PhD student at Vienna University of Technology and works at AIT-Austrian Institute of Technology in Vienna, Austria. His research focuses on optical biosensors and plasmonic nanostructures.

Jakub Dostalek currently serves as senior scientist at AIT-Austrian Institute of Technology in Vienna, Austria. He obtained his PhD degree from Charles University in Prague in 2006 and his research focuses on guided wave optics, plasmonics, optical sensors for medical diagnostics, and polymer-based biointerfaces.